J. Fluid Mech. (2003), *vol.* 491, *pp.* 325–352.
DOI: 10.1017/S0022112003005524 Printed in the United Kingdom

Double-diffusive and Soret-induced convection in a shallow horizontal porous layer

By A. BAHLOUL, N. BOUTANA AND P. VASSEUR

Department of Mechanical Engineering, Ecole Polytechnique, University of Montreal, C.P. 6079, Succ. "Down-Town" Montreal, Quebec, H3C 3A7, Canada
vasseur@meca.polymtl.ca

(Received 31 October 2002 and in revised form 7 May 2003)

This paper reports an analytical and numerical study of the natural convection in a horizontal porous layer filled with a binary fluid. A uniform heat flux is applied to the horizontal walls while the vertical walls are impermeable and adiabatic. The solutal buoyancy forces are assumed to be induced either by the imposition of constant fluxes of mass on the horizontal walls (double-diffusive convection, $a = 0$) or by temperature gradients (Soret effects, $a = 1$). The governing parameters for the problem are the thermal Rayleigh number, R_T, the Lewis number, Le, the solutal Rayleigh number, R_S, the aspect ratio of the cavity, A, the normalized porosity of the porous medium, ε, and the constant a. The onset of convection in the layer is studied using a linear stability analysis. The thresholds for finite-amplitude, oscillatory and monotonic convection instabilities are determined in terms of the governing parameters. For convection in an infinite layer, an analytical solution of the steady form of the governing equations is obtained by assuming parallel flow in the core of the cavity. The critical Rayleigh numbers for the onset of supercritical, R_{TC}^{sup}, or subcritical, R_{TC}^{sub}, convection are predicted by the present theory. A linear stability analysis of the parallel flow pattern is conducted in order to predict the thresholds for Hopf bifurcation. Numerical solutions of the full governing equations are obtained for a wide range of the governing parameters. A good agreement is observed between the analytical prediction and the numerical simulations.

1. Introduction

The study of the onset of linear and nonlinear convection of a single-component flow in a porous medium is a classical subject. A detailed review of the topic is given by Joseph (1976). More recently, the Rayleigh–Bénard convection in a two-components system has received considerable attention. For this situation, where the flows are induced by both temperature and solute fields, the dynamics of heat and mass transfer can be very different from those driven by the temperature field solely. Interest in coupled heat and mass transfer due to buoyancy forces in porous media has been motivated by such diverse engineering problems as the dispersion of chemical contaminants through water-saturated soil, the exploitation of continental geothermal reservoir, the migration of moisture through the air contained in fibrous insulation, metallurgy, electrochemistry, geophysics, etc.

Two kinds of problems have been considered in the literature concerning the convection of a binary mixture filling a horizontal porous layer. The first kind of problem, called double diffusion, considers flows induced by the buoyancy forces

resulting from the imposition of both thermal and solutal boundary conditions on the layer. Early investigations on double-diffusive natural convection in porous media primarily focused on the problem of convective instability in a horizontal layer. To this end Nield (1967), Taunton, Lightfoot & Green (1972), Poulikakos (1986), Taslim & Narusawa (1986) and Malashetty (1993) used linear stability analysis to investigate the onset of thermohaline convection. Criteria for the onset of motion, via stationary and oscillatory modes, were derived by these authors for various conditions. Rudraiah, Shrimani & Fredrich (1982*a*) also used the linear stability theory to predict the region of instability via salt-finger and diffusive regimes for thermohaline convection in a porous layer. Nonlinear thermohaline convection in a porous medium subject to finite-amplitude motion was also considered by these authors (Rudraiah *et al.* 1982*b*). The effects of the governing parameters, on both the Nusselt and Sherwood numbers, were predicted on the basis of a truncated representation of Fourier series. A combined theoretical and numerical study of the mass transfer effected by high-Rayleigh-number Bénard convection was reported by Trevisan & Bejan (1987). The overall mass transfer was predicted by these authors in terms of three distinct scaling laws. Chen & Chen (1993) studied two-dimensional double-diffusive fingering convection in a horizontal porous layer in which periodic conditions were prescribed. The stability boundaries, which separate regions of different types of convective motion (steady fingering, periodic convection, unsteady convection), were identified in terms of the thermal and solutal Rayleigh numbers. Recently, double-diffusive convection in a horizontal porous layer subject to vertical gradients of temperature and solute was investigated by Mamou & Vasseur (1999). Instabilities via stationary and oscillatory modes were determined analytically, on the basis of the linear and nonlinear perturbation theories, in terms of the governing parameters of the problem. The existence of finite-amplitude subcritical convection was predicted by these authors.

The second kind of problem considers thermal convection in a binary fluid driven by Soret effects. For this situation the species gradients are not due to the imposition of solutal boundary conditions as in the case of double diffusion. Rather, they result from the imposition of a temperature gradient in an otherwise uniform-concentration mixture. Brand & Steinberg (1983*a*, *b*) investigated the influence of Soret-induced solutal buoyancy forces on the convective instability of a fluid mixture in a porous medium heated isothermally. Results were obtained by these authors for the onset of motion and in nonlinear convection. It was demonstrated that the governing parameters of the problem can be reduced to a thermal Rayleigh number, R_T, and a buoyancy ratio, φ. It was also found that either a stationary instability or an oscillatory instability can occur as the first bifurcation depending on the sign and magnitude of φ. The same problem was reconsidered by Taslim & Narusawa (1986), taking into account not only the Soret effect but also the Duffour effect (temperature gradients induced by concentration gradients). The Soret effect on the linear stability of a fluid mixture in a porous medium, in the presence of a temperature gradient, was investigated by Ouarzazi & Bois (1994). The temperature gradient was assumed to vary periodically with respect to time. The two-dimensional instability thresholds, for both oscillatory and stationary instabilities, were predicted by these authors. More recently, the onset of Soret-driven convection in an infinite horizontal porous layer heated isothermally from below or from above has been considered by Sovran, Charrier-Mojtabi & Mojtabi (2001). A linear stability analysis was used to predict the onset of motion in terms of the buoyancy ratio, the Lewis number and the normalized porosity of the porous medium. Depending on the value of the separation ratio it

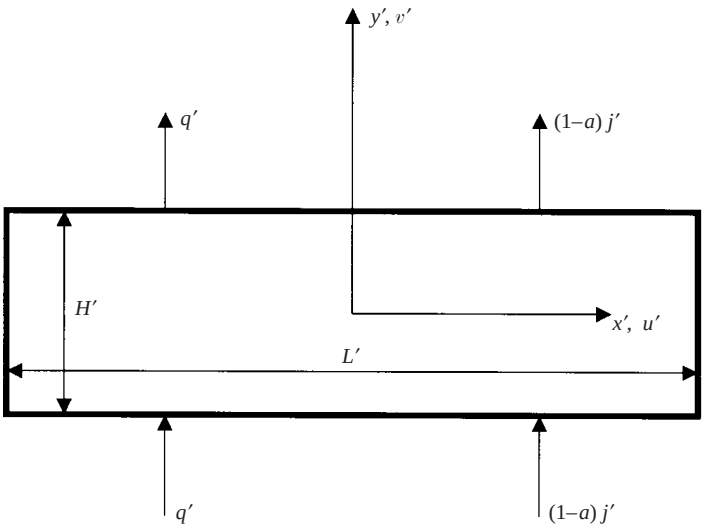

FIGURE 1. Schematic diagram of the physical model and coordinate system.

was found analytically and numerically that the motionless solution loses its stability via stationary or Hopf bifurcations.

In all the above papers, Dirichlet boundary conditions on temperature are imposed on the horizontal boundaries of the system. In the present investigation, the vertical gradients of temperature, and the resulting gradients of solute induced by the Soret effect, result from the imposition of constant fluxes of heat on the horizontal boundaries (Neumann boundary conditions). The layout of the paper is as follows. First, the governing equations describing the physical model considered here are formulated in the next section. Both double-diffusive convection and convection induced by Soret effects will be considered. The numerical procedure used to solve the full governing equations is discussed in § 3.1. A closed-form analytical solution, based on the parallel flow approximation, is presented in § 3.2. Linear stability analyses are carried out in § 4.1 to predict the critical Rayleigh numbers for the onset of motion from the rest state. The stability of the parallel flow regime is investigated numerically and discussed in § 4.2. Finally, concluding remarks are made in § 5.

2. Mathematical formulation of the problem

The configuration considered in this study is a horizontal porous layer of uniform thickness H', width L', permeability K and porosity ϕ filled with a binary fluid (see figure 1). The origin of the coordinate system is located at the centre of the cavity with x' and y' being the horizontal and vertical coordinates, respectively. Neumann boundary conditions are applied, for both temperature and concentration, on the horizontal walls of the layer. All the boundaries are impermeable. The porous medium is considered to be uniform and in local thermal and compositional equilibrium with the fluid. The effects due to viscous dissipation and porous medium inertial forces are assumed to be negligible. The binary fluid is assumed to be Newtonian and to satisfy the Boussinesq approximation. The density variation with temperature and concentration is described by the state equation $\rho = \rho_0[1 - \beta_T(T' - T_0') - \beta_N(N - N_0)]$ where ρ_0 is the fluid mixture density at temperature $T = T_0'$ and mass fraction $N = N_0$ and β_T and β_N are the thermal and concentration expansion coefficients, respectively.

The subscript $_0$ refers to condition at the origin of the coordinate system. The mass fraction of the denser component of the mixture, N_0, is assumed to be initially uniform. The phenomenological equations relating the fluxes of heat $\boldsymbol{Q}'$ and matter $\boldsymbol{J}'$ to the thermal and solute gradients present in a binary fluid mixture are given by (see for instance, De Groot & Mazur 1962)

$$\boldsymbol{Q}' = -k\nabla T', \tag{2.1}$$

$$\boldsymbol{J}'(1-a) = -\rho D\nabla N - a\rho D' N(1-N)\nabla T', \tag{2.2}$$

where a is a real number, the significance of which will be discussed at the end of this section, k and D are the thermal conductivity and the mass diffusivity of species through the fluid-saturated porous medium, and D' is the effect thermal diffusion coefficient.

The equations expressing conservation of momentum, energy and species are given by

$$\nabla^2\Psi' = -\frac{gK\beta_T}{\nu}\frac{\partial}{\partial x'}\left(T' + \frac{\beta_N}{\beta_T}N\right), \tag{2.3}$$

$$(\rho C)_p\frac{\partial T'}{\partial t'} + (\rho C)_f \boldsymbol{V}'\cdot\nabla T' = k\nabla^2 T', \tag{2.4}$$

$$\phi\frac{\partial N}{\partial t'} + \boldsymbol{V}'\cdot\nabla N = D\nabla^2 N + aD'N(1-N)\nabla^2 T', \tag{2.5}$$

where $\boldsymbol{V}'$ is the Darcy velocity, g the gravitational acceleration, ν the kinematic viscosity, $(\rho C)_p$ and $(\rho C)_f$ are respectively the heat capacity of the fluid and the saturated porous medium and Ψ' the stream function. As usual, $u' = \partial\Psi'/\partial y'$ and $v' = -\partial\Psi'/\partial x'$, such that the conservation of mass is satisfied.

The boundary conditions applied on the horizontal boundaries of the system are uniform fluxes of heat and mass per unit area, q' and $(1-a)j'$ respectively. It is assumed that the vertical walls of the cavity are thermally well insulated and impermeable. Thus we have

$$\left.\begin{array}{lll} x' = \pm\dfrac{L'}{2}, & \Psi' = 0, & \dfrac{\partial T'}{\partial x'} = \dfrac{\partial N}{\partial x'} = 0; \\ y' = \pm\dfrac{H'}{2}, & \Psi' = 0, & \dfrac{\partial T'}{\partial y'} = -\dfrac{q'}{k}; \\ & & \dfrac{\partial N}{\partial y'} = \dfrac{j'(1-a)}{\rho D} - a\dfrac{D'}{D}N(1-N)\dfrac{\partial T'}{\partial y'}. \end{array}\right\} \tag{2.6}$$

In general the Soret effect is small and it is assumed that $N(1-N)$ can be approximated by $N_0(1-N_0)$ as discussed for instance by Bergeron *et al.* (1998).

The dimensionless variables (primed quantities are dimensional) are defined as follows:

$$\left.\begin{array}{ll} (x, y) = (x', y')/H', & (u, v) = (u', v')H'/\alpha, \\ t = t'\alpha/H'^2, & \varepsilon = \phi/\sigma, \\ T = (T' - T_0')/\Delta T', & \Delta T' = q'H'/k, \\ \Psi = \Psi'/\alpha, & S = N/\Delta N, \end{array}\right\} \tag{2.7}$$

where $\Delta N = -j'/\rho D$ for double-diffusive convection and $\Delta N = N_0(1-N_0)\Delta T' D'/D$ for Soret-driven convection; $\sigma = (\rho C)_p/(\rho C)_f$ is the heat capacity ratio.

In terms of the above definitions, the dimensionless governing equations are given by

$$\nabla^2\Psi = -\left(R_T\frac{\partial T}{\partial x} + \frac{R_S}{Le}\frac{\partial S}{\partial x}\right), \tag{2.8}$$

$$\frac{\partial T}{\partial t} + u\frac{\partial T}{\partial x} + v\frac{\partial T}{\partial y} = \nabla^2 T, \tag{2.9}$$

$$\varepsilon\frac{\partial S}{\partial t} + u\frac{\partial S}{\partial x} + v\frac{\partial S}{\partial y} = \frac{1}{Le}(\nabla^2 S - a\nabla^2 T). \tag{2.10}$$

The corresponding dimensionless boundary conditions are

$$\left.\begin{aligned} x = \pm\frac{A}{2}, \quad & \Psi = 0, \quad \frac{\partial T}{\partial x} = \frac{\partial S}{\partial x} = 0; \\ y = \pm\frac{1}{2}, \quad & \Psi = 0, \quad \frac{\partial T}{\partial y} = -1; \ \frac{\partial S}{\partial y} = (a-1) + a\frac{\partial T}{\partial y}. \end{aligned}\right\} \tag{2.11}$$

From the above equations it is seen that the present problem is governed by the thermal Rayleigh number R_T, the solutal Rayleigh number R_S, the Lewis number Le, the normalized porosity ε and the cavity aspect ratio A. These parameters are given by

$$\left.\begin{aligned} R_T = \frac{g\beta_T K\Delta T' H'}{\alpha\nu}, \quad & R_S = \frac{g\beta_N K\Delta N H'}{D\nu}, \\ Le = \frac{\alpha}{D}, \quad & A = \frac{L'}{H'}, \quad \varepsilon = \frac{\phi}{\sigma}. \end{aligned}\right\} \tag{2.12}$$

The thermal and solutal Rayleigh numbers R_T and R_S are related by the expression $R_S = R_T\varphi Le$, where φ is the buoyancy ratio defined as

$$\varphi = \frac{\beta_N\Delta N}{\beta_T\Delta T'}. \tag{2.13}$$

In the present study the intensity of the thermal and solutal buoyancy forces are expressed in terms of the parameters R_T and R_S or in terms of R_T and φ.

The heat and solute transports can be expressed in terms of the Nusselt and Sherwood numbers defined respectively as

$$Nu = \frac{1}{\Delta T}, \qquad Sh = \frac{1}{\Delta S}, \tag{2.14}$$

where $\Delta T = T(0,-1/2) - T(0,1/2)$ and $\Delta S = S(0,-1/2) - S(0,1/2)$ are the temperature and concentration differences, evaluated at $x = 0$.

In the above equations the case $a = 0$ corresponds to double-diffusive convection for which the solutal buoyancy forces in the porous layer are induced by the imposition of a constant mass flux q' such that $\partial T/\partial y = -1$ on the horizontal boundaries. According to (2.11) the corresponding solutal boundary conditions are given by $\partial S/\partial y = -1$. On the other hand $a = 1$ corresponds to the case of a binary fluid subject to the Soret effect. For this situation the boundary conditions on concentration result from the fact that the solid boundaries are assumed impermeable ($\boldsymbol{J}' = \mathbf{0}$) such that $(\partial S/\partial y - \partial T/\partial y = 0)$.

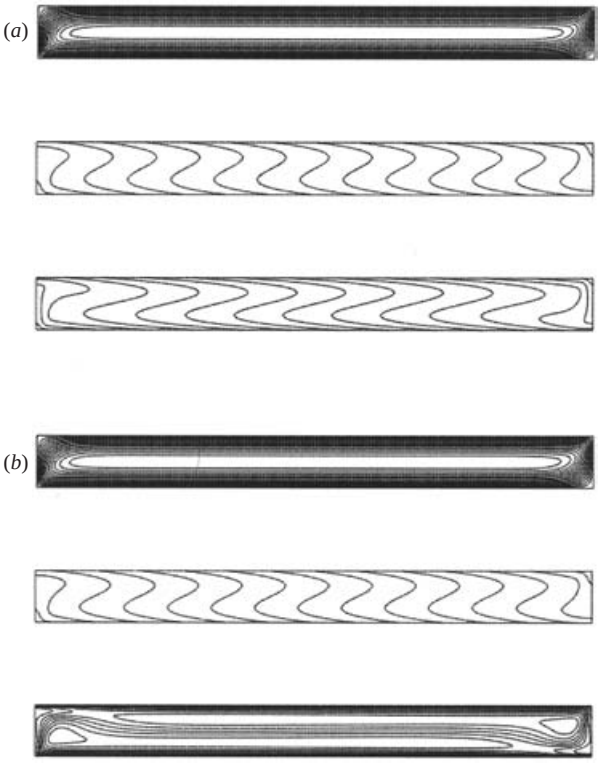

FIGURE 2. Contour lines of stream function (top), temperature (middle) and concentration (bottom) predicted by the numerical solution of the full governing equations for $R_T = 700$, $R_S = -300$, $Le = 2$, $A = 10$, $\varepsilon = 1$. (*a*) Double-diffusive convection $a = 0$, $\Psi_0 = 9.941$, $Nu = 5.483$, $Sh = 5.834$; (*b*) Soret-driven convection $a = 1$, $\Psi_0 = 10.536$, $Nu = 5.531$, $Sh = 6.204$.

3. Finite-amplitude convection

3.1. *Numerical solution*

The numerical solution of governing equations (2.8)–(2.10), with specified boundary conditions (2.11), is obtained using the SIMPLER algorithm (Patankar 1980). The control-volume formulation used in the algorithm ensures continuity of the convective and diffusive fluxes as well as overall momentum and energy conservation. The mesh size required for sufficient numerical accuracy depends mainly on the thermal and solutal Rayleigh numbers and the aspect ratio of the porous layer. The nodal points were skewed in the x- and y-directions to obtain a greater concentration of points near the solid boundaries. Numerical tests, using various mesh sizes, were done for the same conditions in order to determine the best compromise between accuracy of the results and computer time. Besides the usual control, the accuracy of computations was controlled using energy and mass fraction conservation within the system.

Typical numerical results are presented in figure 2(a, b) for $R_T = 700$, $R_S = -300$ ($\varphi = -0.21$), $Le = 2$, $\varepsilon = 1$, $A = 10$ and $a = 0$ (double-diffusive-driven convection) and 1 (Soret-driven convection), respectively. On the graphs streamlines, isotherms and isoconcentrates are presented from top to bottom. The results clearly illustrate the fact that for a shallow cavity ($A \gg 1$) the flow in the core region of the enclosure is essentially parallel while the temperature and concentration in the core are

linearly stratified in the horizontal direction. The analytical solution, developed in the following section, will rely on these observations.

Numerical tests have been performed to determine the minimum aspect ratio above which the flow can be assumed to be parallel. In the range of the parameters considered in this investigation it was found that the numerical results can be considered independent of the aspect ratio when $A \geqslant 8$. For this reason most of the numerical results reported here were obtained for $A = 10$ with typically 60×180 mesh points.

3.2. *Analytical solution*

In general it is not possible to find an analytical solution to the set of equations (2.8)–(2.10) subject to boundary conditions (2.11). However, in the limit of a shallow cavity ($A \gg 1$) it is possible to find approximate solutions (see for instance Bejan & Tien 1978; Walker & Homsy 1978; Blythe, Daniels & Simpkins 1985; Daniels, Simpkins & Blythe 1989). In the present study the parallel flow approximation, as discussed for instance by Mamou *et al.* (1995), is adopted. Thus, when A is sufficiently large, as illustrated by the numerical results (see for instance figure 2), the flow in the central part of the cavity is essentially parallel such that $\Psi(x, y) = \Psi(y)$ for which both $\partial T/\partial x$ and $\partial S/\partial x$ are a function of y only. This leads to the following simplifications:

$$\Psi(x, y) = \Psi(y), \quad T(x, y) = C_T x + \theta_T(y), \quad S(x, y) = C_S x + \theta_S(y). \tag{3.1}$$

Using these approximations together with the boundary conditions (2.11), the steady form of (2.8)–(2.10) is reduced to a set of ordinary differential equations, which can be solved to yield the following closed-form analytical solution:

$$\Psi = \Psi_0(1 - 4y^2), \tag{3.2}$$

$$\theta_T = \frac{C_T \Psi_0}{3}(3y - 4y^3) - y, \tag{3.3}$$

$$\theta_S = \frac{(LeC_S + aC_T)\Psi_0}{3}(3y - 4y^3) - y, \tag{3.4}$$

where

$$\Psi_0 = \bar{R}_T(C_T + \varphi C_S), \quad \bar{R}_T = R_T/R^{sup}, \quad R^{sup} = 12. \tag{3.5}$$

The equations for C_T and C_S can be established by imposing zero heat and mass transfer across any transversal section, which yields

$$C_T = \frac{4b\Psi_0}{3\left(2b + \Psi_0^2\right)}, \tag{3.6}$$

$$C_S = \frac{-3aC_T\left(Le\Psi_0^2 - (1 - 1/Le)b\right) + 4b\Psi_0 Le}{3\left(2b + Le^2\Psi_0^2\right)}, \tag{3.7}$$

where $b = 15/16$.

Combining the expressions for C_T and C_S, (3.6) and (3.7), with the expression for Ψ_0 it is found that

$$\Psi_0\left(Le^4\Psi_0^4 - 2bLe^2 d_1\Psi_0^2 - b^2 d_2\right) = 0, \tag{3.8}$$

where

$$\left.\begin{aligned} d_1 &= \bar{R}_T Le[Le + \varphi(1 - a)] - (Le^2 + 1), \\ d_2 &= 4\bar{R}_T Le^2[1 + \varphi(Le + a)] - 4Le^2. \end{aligned}\right\} \tag{3.9}$$

From the above results it follows that the solution for Ψ_0 is

$$\Psi_0 = 0 \tag{3.10}$$

or

$$\Psi_0 = \pm\frac{\sqrt{b}}{Le}\left(d_1 \pm \sqrt{d_1^2 + d_2}\right)^{1/2}. \tag{3.11}$$

The local heat and mass transfer rates are given, according to (2.14), (3.3) and (3.4), by

$$Nu = 6\left(\frac{\Psi_0^2 + 2b}{\Psi_0^2 + 12b}\right), \qquad Sh_0 = 6\left(\frac{Le^2\Psi_0^2 + 2b}{Le^2\Psi_0^2 + 12b}\right), \qquad Sh = \frac{Sh_0}{1 + Sh_0(Nu - 1)/Nu}, \tag{3.12}$$

where Sh_0 and Sh are the local mass transfer rates for double diffusion ($a = 0$) and Soret effect ($a = 1$), respectively.

Equations (3.10) and (3.11) indicate that five different steady-state solutions are predicted by the present analytical model. The first one, (3.10), corresponds to the rest state. The first signs + and − in (3.11) indicate counterclockwise and clockwise unicellular circulations, respectively. Within the brackets the + and − signs refer to stable and unstable convection flows respectively.

The transition from the rest state ($\Psi_0 = 0$) to convection ($\Psi_0 \neq 0$) is also predicted by the present analytical model. From (3.11) it is seen that two types of bifurcations are possible. The first one is the classical supercritical bifurcation characterized by a transition from the quiescent state to the convective regime occurring through zero flow amplitude.

The threshold, expressed in terms of the supercritical Rayleigh number R_{TC}^{sup}, is obtained when the conditions $d_1 < 0$ and $d_2 = 0$ are satisfied, as

$$R_{TC}^{sup} = \frac{R^{sup}}{[1 + \varphi(Le + a)]} \qquad \text{or} \qquad R_{TC}^{sup} = R^{sup} - R_S(1 + a/Le) \tag{3.13}$$

in terms of φ and R_S, respectively.

In the following discussion note that the case $a = 0$ (double-diffusive convection) has been investigated in detail recently by Mamou & Vasseur (1999). Thus the results reported here, for this situation, are not new but are used only for comparison with those for Soret-driven convection.

The case of pure thermal convection ($\varphi = 0$, $a = 0$) will be discussed first. This situation, presented in figures 3 and 4 for comparison purpose, corresponds to a classical Bénard situation. It gives rise to a pitchfork bifurcation occurring at a supercritical Rayleigh number $R_{TC}^{sup} = 12$, as predicted by (3.13). Due to the thermal boundary conditions considered here (Neumann), convection gives rise to a unicellular cell rotating randomly clockwise or conterclockwise. The corresponding variation of the heat (Nu) and mass (Sh) transfer with the thermal Rayleigh number R_T is also presented. The analytical solution, predicted by the present theory, represented by the solid (stable) and dashed (unstable) lines, is observed to be in very good agreement with the numerical results depicted by symbols.

The way that this pitchfork bifurcation is affected by the presence of solutal buoyancy forces is depicted in figures 3 and 4 for the case $Le = 2$. Here again the agreement between the analytical and the numerical results is seen to be excellent in the range of the parameters considered. Figure 3(a–c) illustrates typical results obtained for $\varphi > 0$, namely $\varphi = 0.5$, for which the thermal and solutal buoyancy

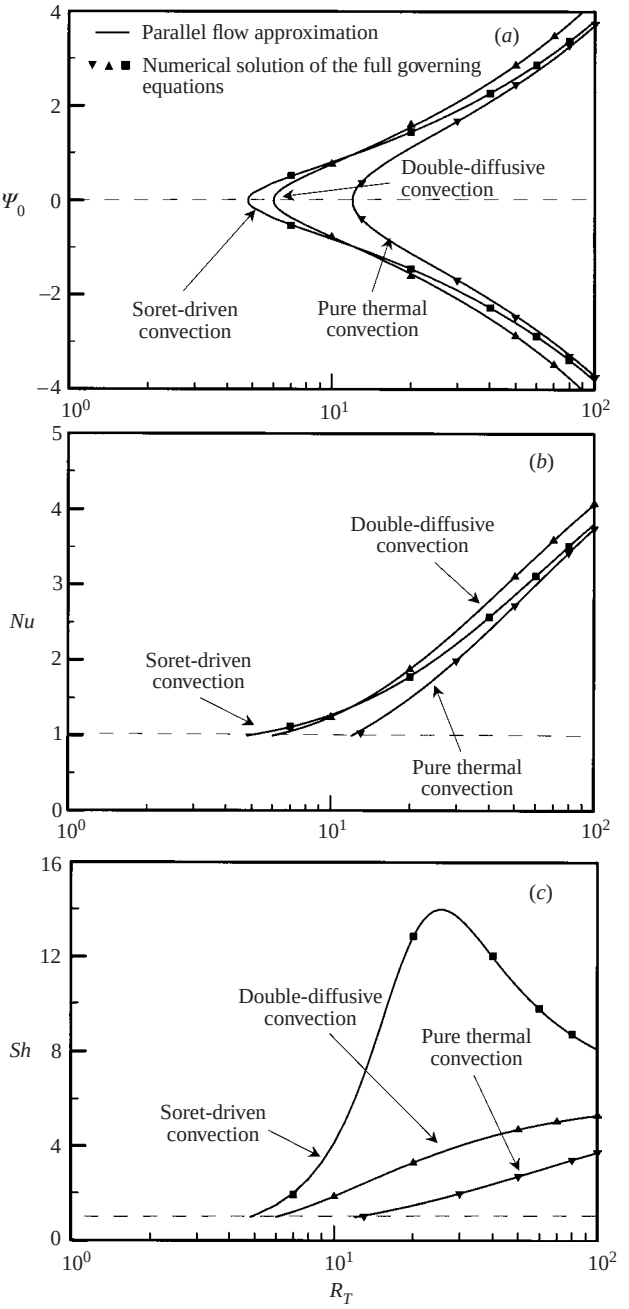

FIGURE 3. Bifurcation diagram in terms of (*a*) Ψ_0, (*b*) *Nu*, (*c*) *Sh*, versus R_T for $a = 0$ and 1, $Le = 2$ and $\varphi = 0.5$.

forces are destabilizing. For this situation, pitchfork bifurcation curves are also obtained for both double-diffusive convection ($a = 0$) and Soret-induced convection ($a = 1$). However, the corresponding supercritical Rayleigh numbers, $R_{TC}^{sup} = 6$ and 4.8 respectively, are lower than the value $R_{TC}^{sup} = 12$ obtained when the layer is destabilized only by the thermal buoyancy forces. It is observed from figure 3(*a*) that, in the range

between the thermal and thermo-solutal thresholds, the magnitude of the resulting flow Ψ_0 is relatively low. On the other hand the flow intensity increases strongly as the value of R_T is made larger than the pure thermal threshold. Figure 3(b) indicates that Nu is greater for double-diffusive convection than for Soret-induced convection. This follows from the fact that the strength of convection is higher for $a=0$ than for $a=1$ as illustrated in figure 3(a). On the other hand the Sherwood number Sh (figure 3c) is observed to be considerably higher in the case of Soret-induced convection.

Figure 4(a–c) shows the values for Ψ_0, Nu and Sh obtained for $\varphi = -0.5$, i.e. when the thermal and solutal buoyancy forces are opposing each other. For this situation, it is well known (see Mamou & Vasseur 1999 for instance), that under appropriate conditions ($R_T > 0$ and $R_S = R_T \varphi Le < 0$) and when the stabilizing agent is the slower diffusing component, i.e. $Le \geqslant 1$, or vice versa, convection takes place through a subcritical bifurcation. The onset of convection occurs with a finite-amplitude convection of magnitude $\Psi_0 = \pm\sqrt{bd_1}/Le$. The subcritical Rayleigh number R_{TC}^{sub} is obtained from the condition $d_1 > 0$ and $d_1^2 + d_2 = 0$ as

$$R_{TC}^{sub} = \frac{(1+Le)R^{sup}}{Le[Le+\varphi(1-a)]^2}[(Le-1)(Le-\varphi) - a\varphi(Le+1) + 2\sqrt{\varphi Le(Le+a-1)(a\varphi - Le+1)}] \quad (3.14a)$$

or, in terms of R_S, as

$$R_{TC}^{sub} = \frac{R_S(a-1) - R^{sup}(1-Le^2) + 2\sqrt{R_S R^{sup}[1-Le^2-a(1+Le)]}}{Le^2}. \quad (3.14b)$$

From the above equations it can be easily demonstrated that the conditions

$$\bar{R}_S < 0 \qquad \text{or} \qquad \varphi < -\frac{1}{Le(1-a)+(Le+a)(Le^2+1)} \quad (3.15a)$$

and

$$Le > \sqrt{(1-a) - \frac{1}{\bar{R}_S}} \quad (3.15b)$$

must be satisfied for the existence of subcritical convection. In the above equations $\bar{R}_S = R_S/R^{sup}$.

For the Lewis number considered in the graphs the subcritical Rayleigh numbers for the onset of the convection are $R_{TC}^{sub} = 36$ for $a=0$ and $R_{TC}^{sub} = 33.59$ for $a=1$. The analytical solution also predicts the existence of an unstable branch (dashed line) connecting the supercritical Rayleigh number $R_{TC}^{sup} \to \infty$, (3.13). The results obtained for $R_T < 0$, corresponding to the case of a layer heated from the top, are also presented in figure 4. For this situation, convection occurs through a pitchfork bifurcation at a supercritical Rayleigh number $R_{TC}^{sup} = -24$, according to (3.13).

Figure 5(a, b) exemplifies the effect of buoyancy ratio φ and Lewis number Le on the value of the stream function at the centre of the cavity Ψ_0 for $R_T = 30$ and 100 respectively. In figure 5(a) the case $\varphi = 0$ corresponds to convection induced solely by the thermal effects for which Ψ_0 is the same for $a = 0$ and $a = 1$. For the case of cooperative solutal and thermal buoyancy forces ($\varphi > 0$) it is observed that, as expected, the strength of the convective flow is promoted by an increase of φ. This follows from the fact that increasing φ, for a fixed value of R_T (i.e. a given strength of the thermal buoyancy forces), increases the total buoyancy forces. Naturally, the

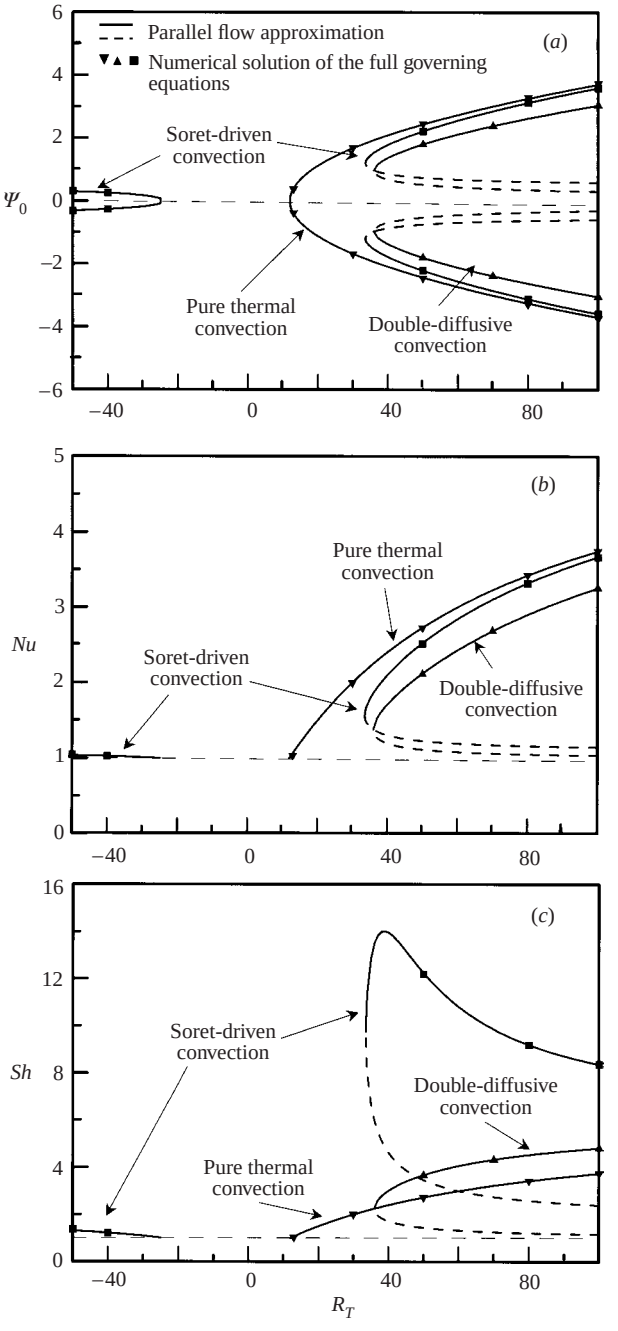

FIGURE 4. As figure 3 but for $\varphi = -0.5$. Dashed lines denote unstable solutions.

opposite effect is observed for the case of opposite solutal and thermal buoyancy forces ($\varphi < 0$). In fact, convection is possible only down to a subcritical buoyancy ratio ($\varphi_c^{sub} = -0.41$ for $a = 0$ and $a = 1$). Below these values the rest state prevails. According to the present theory, for $R_T = 30$ and $Le = 2$ the supercritical buoyancy ratios are $\varphi_c^{sup} = -0.30$ for $a = 0$ and $\varphi_c^{sup} = -0.20$ for $a = 1$ respectively. This situation

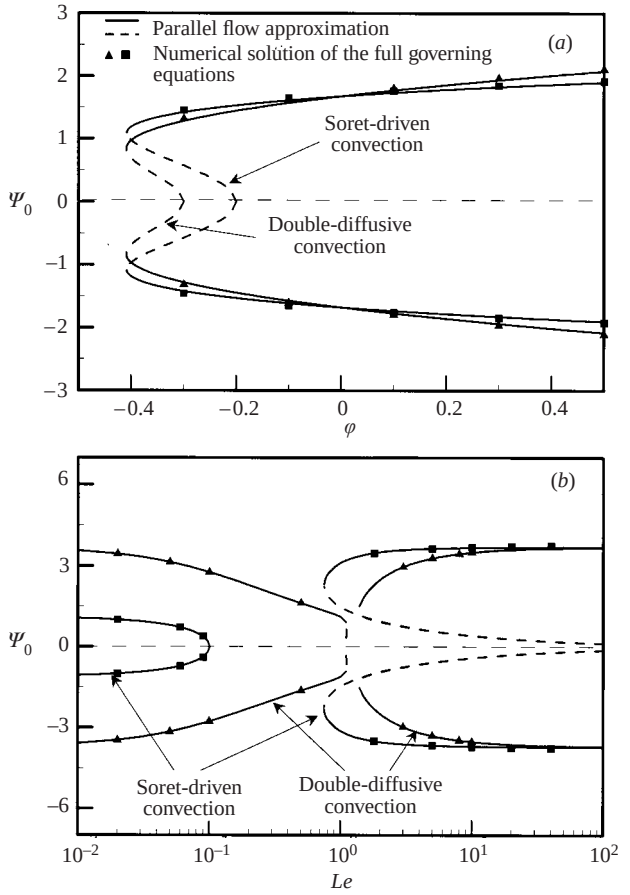

FIGURE 5. Bifurcation diagram for $a = 0$ and 1 for (a) Ψ_0 versus φ for $R_T = 30$ and $Le = 2$; (b) Ψ_0 versus Le for $R_T = 100$ and $\varphi = -0.8$.

gives rise to the existence of a hysteresis loop, the path of which has been described by many authors (Platten & Legros 1984).

The effects of the Lewis number on Ψ_0 are depicted in figure 5(b) for the case $R_T = 100$ and $\varphi = -0.8$ for which the buoyancy forces resulting from the stabilizing agent (mass) are approximately equal and opposite to those from the destabilizing one. The results obtained for double-diffusive convection will be discussed first. For the parameters considered here subcritical convection is possible for $1.11 < Le < 1.38$, while a pure diffusive state prevails between these values. Upon increasing or decreasing Le above or below the threshold Lewis numbers it is seen that Ψ_0 increases asymptotically towards a constant value. In the case of Soret-induced convection a saddle-node bifurcation occurs at $Le = 0.75$. Upon decreasing Le below this value the fluid remains at rest down to $Le = 0.1$ at which a pitchfork bifurcation occurs. On the other hand for $Le > 0.75$ it is found that Ψ_0 increases quickly and tends toward the asymptotic value obtained for double-diffusive convection.

It can be easily demonstrated that, for high Lewis numbers, the present theory yields the same results for double-diffusive and Soret-induced convection (i.e. is independent

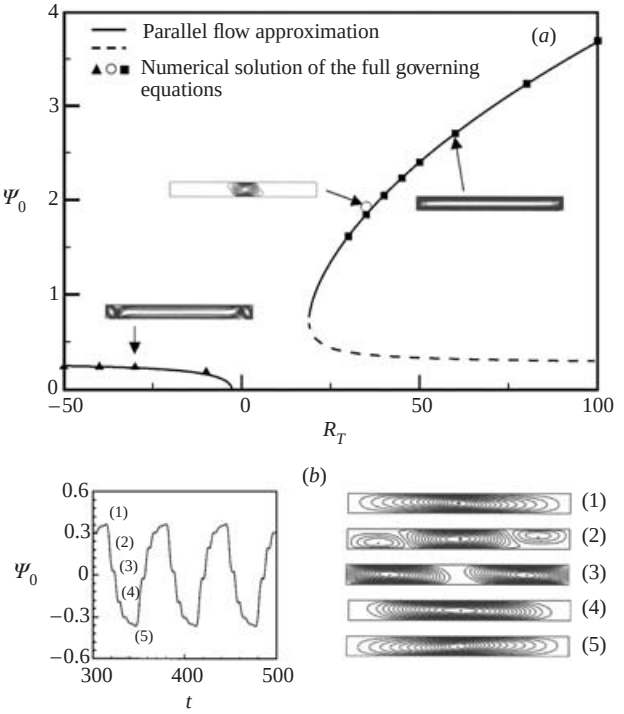

FIGURE 6. (*a*) Bifurcation diagram in terms of Ψ_0 versus R_T for $Le = 10$, $\varphi = -0.5$ and $a = 1$. (*b*) Time evolution of flow structure in half a period for $R_T = 30$.

of *a*). Thus, for $Le \gg 1$, it is found from (3.13) that

$$\Psi_0 \approx \pm 2\sqrt{b}(\bar{R}_T - 1). \tag{3.16}$$

Also it may be shown that the critical Rayleigh numbers for the onset of convection are given by

$$R_T^{sup} = \frac{R^{sup}}{\varphi Le}, \qquad R_T^{sub} = \frac{R^{sup}}{\varphi Le}[1 + 2\sqrt{-\varphi/Le}]. \tag{3.17}$$

Another effect of the Lewis number is illustrated on figures 4(*a*) and 6. These graphs show Ψ_0 versus R_T for $\varphi = -0.5$, $a = 1$ and $Le = 2$ and 10 respectively. All the numerical results obtained for $Le = 2$, figure 4(*a*), correspond to the case of a unicellular flow configuration. For $Le = 10$, figure 6(*a*) indicates the existence of other types of flow configurations. Thus for $R_T < 0$, i.e. in the case of a layer heated from the bottom, the flow pattern consists of two small vortices in the vicinity of the vertical walls of the enclosure and a large cell in the core of the cavity. The strength of convection of the main cell is observed to be in good agreement with the parallel flow model. For $R_T > 0$, the numerical code shows that the flow is parallel in the range $40 < R_T < 100$. However, for $R_T = 35$, it was found that two solutions are possible. Thus, a parallel flow solution can be obtained using another parallel flow configuration as initial conditions. The other solution, consisting of a small vortex located at the centre of the layer, was obtained using the three-cellular flow configuration corresponding to $R_T < 0$, as initial conditions. Finally, it was found that in the vicinity of the subcritical Rayleigh number, $R_{TC}^{sub} = 18.94$, the numerical solution obtained for a layer with a given aspect ratio is not in agreement with the analytical

model ($A \gg 1$). Thus, for $R_T = 30$, the flow is oscillating as illustrated on figure 6(b) where the flow configuration is given for various time steps. Naturally, this behaviour cannot be predicted by the analytical model obtained by solving the steady-state form of the governing equations. Also, for $R_T < 25$, the rest state is predicted by the numerical code. However, the subcritical Rayleigh number R_{TC}^{sub} for the occurrence of finite-amplitude convection depends upon the aspect ratio A of the cavity. Thus, in the vicinity of the turning point, the behaviour of the analytical solution ($A \gg 1$) is not expected to be exactly the same as that predicted by the numerical solution ($A = 10$).

4. Linear stability analysis

In this section the stability both of the rest state and of the convective flows, predicted by the parallel flow approximations, is investigated using the linear stability analysis.

4.1. *Stability of the rest state*

The procedure for the linear stability analysis has been discussed in detail by many authors and in particular by Poulikakos (1986) for the problem of double diffusion in a horizontal porous layer. Therefore, only the main points of the mathematical steps that lead to the solution of the problem are presented here.

The stability to small perturbations from the quiescent state ($\Psi_C = 0,\ T_C = S_C = -y$) of the physical situation described by (2.8)–(2.10) is examined now. In order to do so, it is convenient to rewrite the governing equations using $\tilde{\Psi} = \Psi - \Psi_C$, $\tilde{\Theta} = T - T_C$ and $\tilde{\Phi} = S - S_C$. As usual, the perturbed solution is assumed to have the following functional form:

$$\left.\begin{aligned} \tilde{\Psi}(t, x, y) &= \Psi_0\, \mathrm{e}^{pt} F(x, y), \\ \tilde{\Theta}(t, x, y) &= \Theta_0\, \mathrm{e}^{pt} G(x, y), \\ \tilde{\Phi}(t, x, y) &= \Phi_0\, \mathrm{e}^{pt} G(x, y), \end{aligned}\right\} \tag{4.1}$$

where p is the growth rate of the perturbation, F and G are space functions satisfying the boundary conditions given by (2.11), and Ψ_0, Θ_0 and Φ_0 are small constant amplitudes.

Introducing (4.1) into (2.8)–(2.10) and neglecting second higher-order nonlinear terms yields the following linear system:

$$\Psi_0 \nabla^2 F = -\left(R_T \Theta_0 + \frac{R_S}{Le} \Phi_0 \right) \frac{\partial G}{\partial x}, \tag{4.2}$$

$$p\Theta_0 G + \Psi_0 \frac{\partial F}{\partial x} = \Theta_0 \nabla^2 G, \tag{4.3}$$

$$p\varepsilon \Phi_0 G + \Psi_0 \frac{\partial F}{\partial x} = \frac{1}{Le} (\Phi_0 - a\Theta_0) \nabla^2 G. \tag{4.4}$$

Upon using the weak Galerkin formulation the following set of ordinary differential equations is obtained:

$$\mathscr{K}_\Psi \Psi_0 = \mathscr{B} \left(R_T \Theta_0 + \frac{R_S}{Le} \Phi_0 \right), \tag{4.5}$$

$$p\mathscr{M}\Theta_0 + \mathscr{L}\Psi_0 = -\mathscr{K}\Theta_0, \tag{4.6}$$

$$p\varepsilon\mathscr{M}\Phi_0 + \mathscr{L}\Psi_0 = -\frac{\mathscr{K}}{Le} (\Phi_0 - a\Theta_0), \tag{4.7}$$

where

$$\left.\begin{aligned} &\mathscr{K}_{\psi} = \int_{\Omega} (\nabla F)^2 \, \mathrm{d}\Omega, \quad \mathscr{B} = \int_{\Omega} \frac{\partial G}{\partial x} F \, \mathrm{d}\Omega, \quad \mathscr{K} = \int_{\Omega} (\nabla G)^2 \, \mathrm{d}\Omega, \\ &\mathscr{L} = \int_{\Omega} \frac{\partial F}{\partial x} G \, \mathrm{d}\Omega, \qquad \mathscr{M} = \int_{\Omega} G^2 \, \mathrm{d}\Omega, \end{aligned}\right\} \tag{4.8}$$

Ω being the physical domain of integration.

Substituting (4.5) and (4.6) into (4.7) we readily arrive at the dispersion relationship:

$$\varepsilon^2 Le^2 p^2 - \gamma \varepsilon Le p_1 p - \gamma^2 p_2 = 0, \tag{4.9}$$

where

$$\left.\begin{aligned} &p_1 = Le \bar{R}_T (\varepsilon + \varphi) - (1 + \varepsilon Le), \\ &p_2 = \varepsilon Le (\bar{R}_T [1 + \varphi (Le + a)] - 1), \\ &R^{sup} = \frac{\mathscr{K}_{\psi} \mathscr{K}}{\mathscr{B} \mathscr{L}}, \qquad \gamma = \frac{\mathscr{K}}{\mathscr{M}}. \end{aligned}\right\} \tag{4.10}$$

Solving (4.9) for p it is found that

$$p = \frac{\gamma}{2\varepsilon Le} \left(p_1 \pm \sqrt{p_1^2 + 4p_2} \right) \tag{4.11}$$

where, in general, the constant p is a complex number which can be decomposed as $p = p_r + \mathrm{i} p_i$, where p_r and p_i are the real and imaginary parts respectively. From (4.11) it is observed that

$$\left.\begin{aligned} &p_r = \frac{\gamma}{2\varepsilon Le} \left(p_1 \pm \sqrt{p_1^2 + 4p_2} \right) \\ &p_i = 0 \end{aligned}\right\} \quad \text{if} \quad p_1^2 + 4p_2 \geqslant 0,$$

$$\left.\begin{aligned} &p_r = \frac{\gamma}{2\varepsilon Le} p_1 \\ &p_i = \pm \frac{\gamma}{2\varepsilon Le} \sqrt{|p_1^2 + 4p_2|} \end{aligned}\right\} \quad \text{if} \quad p_1^2 + 4p_2 < 0. \tag{4.12}$$

The marginal state of instability corresponds to $p = 0$ (i.e. $p_2 = 0$), from which the supercritical Rayleigh number for the onset of supercritical convection, R_{TC}^{sup}, is given by

$$R_{TC}^{sup} = \frac{R^{sup}}{[1 + \varphi (Le + a)]} \qquad \text{or} \qquad R_{TC}^{sup} = R^{sup} - R_S (1 + a/Le). \tag{4.13}$$

The above result is similar to that predicted by the parallel flow theory, (3.13).

The marginal state of instability at which oscillatory convection may arise corresponds to $p_1 = 0$, from which the overstable critical Rayleigh number, R_{TC}^{over}, is obtained as

$$R_{TC}^{over} = \frac{(\varepsilon Le + 1)}{Le(\varepsilon + \varphi)} R^{sup} \qquad \text{or} \qquad R_{TC}^{over} = \frac{(1 + \varepsilon Le) R_{sup} - R_S}{\varepsilon Le}. \tag{4.14}$$

The oscillatory regime exists only when the condition $p_1^2 + 4p_2 < 0$ is satisfied, i.e. $R_{TC}^{over} < R_T < R_{TC}^{osc}$, where the value of R_{TC}^{osc} is deduced from the condition $p_1^2 + 4p_2 = 0$

as

$$\left.\begin{aligned} R_{TC}^{osc} &= \frac{(\varepsilon Le-1)(\varepsilon-\varphi)-2a\varepsilon\varphi+2\sqrt{-\varepsilon\varphi[\varepsilon(Le+a)-1][\varepsilon Le-\varphi a-1]}}{Le(\varepsilon+\varphi)^2}R^{sup} \\ \text{or} \\ R_{TC}^{osc} &= \frac{(\varepsilon Le-1)R^{sup}-R_S+2\sqrt{[1-\varepsilon(Le+a)]R_S R^{sup}}}{\varepsilon Le}. \end{aligned}\right\} \tag{4.15}$$

At the onset of oscillatory flow the value of the frequency p_i is given, according to (4.12) and (4.14), by

$$p_i = \pm\frac{\gamma}{\sqrt{\varepsilon}Le}\sqrt{\left|\frac{1+\varphi[(\varepsilon Le+1)(Le+a)-Le]}{\varepsilon+\varphi}\right|} \tag{4.16}$$

from which the period of oscillation $T = 2\pi/p_i$ can be evaluated.

The range of possible oscillations can be deduced from the above equation as

$$-\varepsilon < \varphi < -[\varepsilon Le^2 + a(\varepsilon Le+1)]^{-1}. \tag{4.17}$$

Assuming that the Lewis number characterizing the binary fluid is large ($Le \gg 1$), it follows from (4.16) that

$$T = \frac{2\pi}{\gamma}\left|\frac{\varphi+\varepsilon}{\varphi}\right|^{1/2}. \tag{4.18}$$

In the above equations the values of R_{TC}^{sup} and γ depend only on the aspect ratio of the enclosure A and on the thermal and solutal boundary conditions imposed on the system. In general, these parameters have to be evaluated numerically. However, with the present boundary conditions, an analytical solution is possible.

As discussed by Mamou & Vasseur (1999) it can be demonstrated that, when constant fluxes of heat and solute are imposed on the horizontal walls of the system, the functions $F(x, y)$ and $G(x, y)$, in (4.1), are given by

$$\left.\begin{aligned} F(x,y) &= \cos(\pi x/4)[\cosh(\xi_0 y) - \gamma_0\cos(\eta_0 y)], \\ G(x,y) &= \sin(\pi x/4)[\cosh(\xi_0 y) + \gamma_0\cos(\eta_0 y)], \end{aligned}\right\} \tag{4.19}$$

where γ_0, ξ_0 and η_0 are defined as

$$\xi_0 = \sqrt{\frac{\pi}{A}\left(\sqrt{R^{sup}}+\frac{\pi}{A}\right)}, \quad \eta_0 = \sqrt{\frac{\pi}{A}\left(\sqrt{R^{sup}}-\frac{\pi}{A}\right)}, \quad \gamma_0 = \frac{\cosh(\xi_0/2)}{\cos(\eta_0/2)} \tag{4.20}$$

and R^{sup} is a constant which can be computed from the relation

$$\xi_0\tanh(\xi_0/2) = \eta_0\tan(\eta_0/2). \tag{4.21}$$

Introducing (4.10) and (4.20) into (4.8), and performing the resulting integration, it is found that

$$\gamma = \frac{\mathscr{K}}{\mathscr{M}} = \frac{\pi\sqrt{R^{sup}}\left(a_1-\gamma_0^2 a_3\right)/2}{\left(a_1+2\gamma_0 a_2+\gamma_0^2 a_3\right)(A/2)} \tag{4.22}$$

where

$$\left.\begin{aligned} a_1 &= \tfrac{1}{2}[A+\sinh(\xi_0 A)/\xi_0], \quad a_2 = \frac{4\xi_0}{\xi_0^2+\eta_0^2}\sinh(\xi_0 A/2)\cos(\eta_0 A/2), \\ a_3 &= \tfrac{1}{2}[A+\sin(\xi_0 A)/\eta_0]. \end{aligned}\right\} \tag{4.23}$$

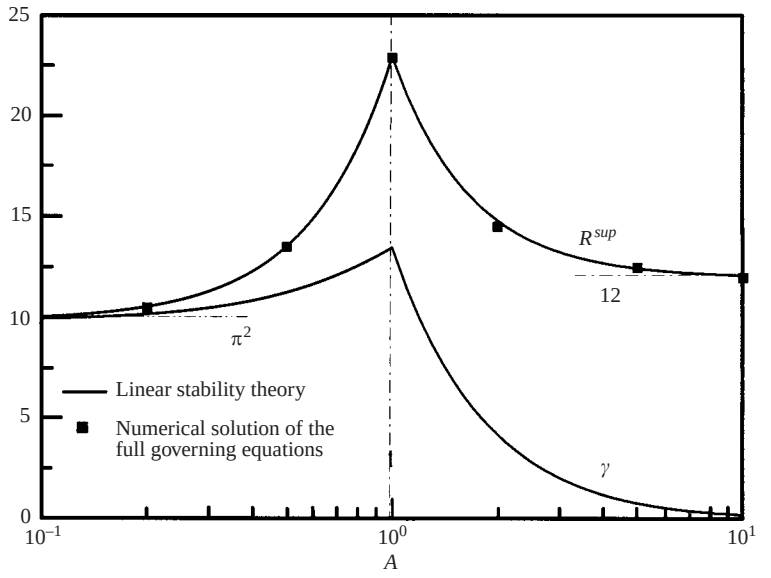

FIGURE 7. Parameters R^{sup} and γ as a function of the aspect ratio A.

The above equations for γ and R^{sup} can be solved numerically for a given value of the aspect ratio A of the layer. The results are presented in figure 7. It is noted that both R^{sup} and γ are maximum when $A = 1$. Thus, $R^{sup} = 22.9$ for a square cavity, $R^{sup} \to \pi^2$ for $A \to 0$, and $R^{sup} \to 12$ as $A \to \infty$. This last result is in agreement with the prediction of the parallel flow approximation, (3.13). The value of R^{sup} can also be evaluated indirectly from the numerical procedure described in § 3.1. Thus, for a given set of the governing parameters, the supercritical Rayleigh R_{TC}^{sup} for the onset of convection can be estimated numerically, yielding the value of R^{sup}, through (4.13). The numerical results obtained in this way, for a few values of A, are depicted in figure 7. They are seen to be in excellent agreement with the prediction of (4.21). Also, the graph indicates that the value of γ, which is linearly related to the perturbation amplitude growth parameter p, (4.11), decreases towards zero when A is sufficiently large. Thus, for an infinite layer, the amplitude perturbation growth rate is expected to be very small.

The influence of the buoyancy ratio φ and porosity ε on the period of oscillation T, at the onset of overstable convection, is illustrated in figure 8 for the case $Le = 2$. The results indicate that, for a given value ε, the range of φ for the occurrence of oscillatory instability is larger for the Soret case than for the double-diffusive one. Also the range of φ decreases considerably as the value of ε is made smaller. Numerical confirmation of the linear stability theory is also indicated in the graph for the case $\varphi = 0.8$.

Figure 9(a) shows the numericals results obtained, using the rest state as initial conditions ($\Psi = 0, T = S = -y$) together with a small-amplitude perturbation ($\Psi_0 = 10^{-6}$), for the case $R_T = 300$, $Le = 2$, $\varphi = -0.8$, $\varepsilon = 1$, $A = 1$ and $a = 1$. It is found that, at the beginning of the convective motion, the flow oscillates with a period $T = 0.205$, this result being in excellent agreement with the value $T = 0.197$ predicted by the linear stability theory. However, as the time is increased, it is found numerically that, due to the fact that the advection (nonlinear) effects become more and more

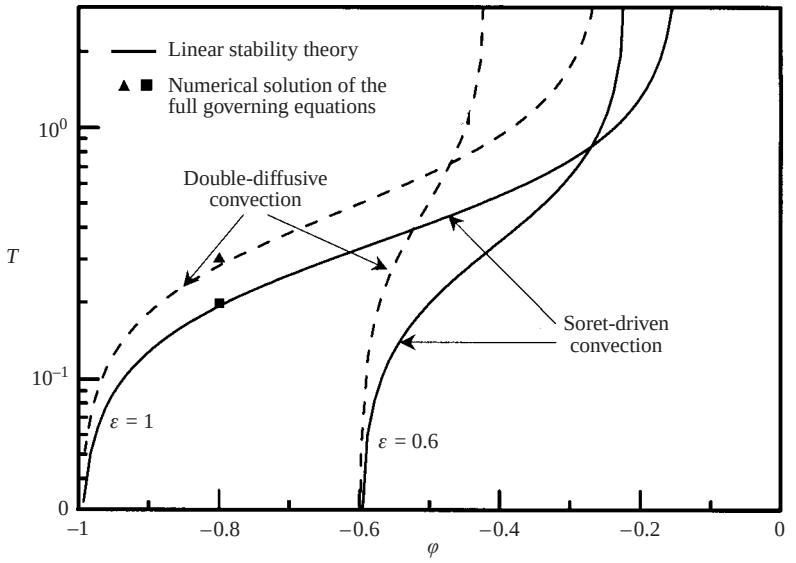

FIGURE 8. Period of oscillation T as a function of φ and ε for the case $Le = 2$.

important, the system converges towards a finite-amplitude convective steady state. The evolution of the flow pattern during half a period is presented in figure 9(*b*).

The reduced Rayleigh numbers ($\bar{R}_{TC} = R_{TC}/R^{sup}$), (4.13), (4.14) and (4.15), are plotted in figure 10 as a function of φ for the case $a = 1$, $\varepsilon = 0.8$ and $Le = 2$. The $(\bar{R}_{TC}, \varphi)$-plane is divided in four quadrants, I (II) correspond to $\varphi > 0$ and $\bar{R}_{TC} > 0$ ($\bar{R}_{TC} < 0$) and IV (III) to $\varphi < 0$ and $\bar{R}_{TC} > 0$ ($\bar{R}_{TC} < 0$). With the thermal boundary conditions considered here it clear that $\bar{R}_{TC} > 0$ ($\bar{R}_{TC} < 0$) corresponds to the case of a layer heated from below (above). Also, it is noted that for $\varphi > 0$ both the thermal and solutal buoyancy forces are cooperative while for $\varphi < 0$ they are opposing each other.

As discussed by Platten & Legros (1984) the physical meaning of φ can be deduced from the linear equation of state. For the rest state, it is readily found that

$$\frac{\partial \rho}{\partial y} = \rho_0 \beta_T \Delta T (1 + \varphi) \tag{4.24}$$

such that $\varphi = -1$ corresponds to neutral buoyancy $\partial\rho/\partial y = 0$. Furthermore, $\partial\rho/\partial y$ has the sign (minus the sign) of ΔT if $\varphi > -1$ ($\varphi < -1$).

The linear stability theory predicts the existence of other characteristic buoyancy ratios. Thus, the poles of critical Rayleigh numbers, (4.13) and (4.14), yield respectively the following two buoyancy ratios:

$$\varphi_1 = -\varepsilon, \qquad \varphi_2 = -(Le + a)^{-1}. \tag{4.25}$$

Also, it can be easily demonstrated that, in the (φ, Le)-plane the intersection of the curves R_{TC}^{sup}, R_{TC}^{over} and R_{TC}^{osc} occurs at a characteristic buoyancy ratio φ_3 given by

$$\varphi_3 = -[\varepsilon Le^2 + a(\varepsilon Le + 1)]^{-1}, \tag{4.26}$$

while the intersection of the curves R_{TC}^{sub} and R_{TC}^{sup} corresponds to

$$\varphi_4 = -[a(Le^2 + Le + 1) + Le^3]^{-1}. \tag{4.27}$$

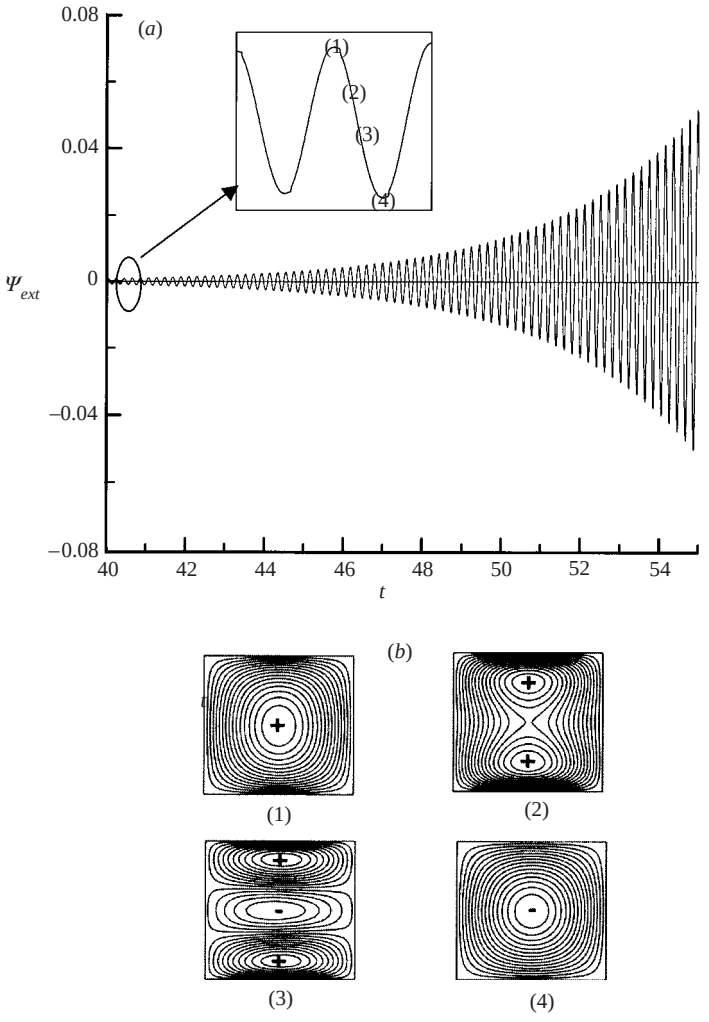

FIGURE 9. (*a*) Time history of the stream function extrema obtained for $R_T = 300$, $\varphi = -0.8$, $Le = 2$, $\varepsilon = 1$, $A = 1$ and $a = 1$. (*b*) Time evolution of flow structure: (1) $t = 41.262$, (2) $t = 41.296$, (3) $t = 41.330$, (4) $t = 41.364$.

The four buoyancy ratios ($\varphi_1, \varphi_2, \varphi_3, \varphi_4$), given by (4.25)–(4.27), together with the value $\varphi_0 = -1$ resulting from (4.24), are indicated in figure 10 for convenience. The case of a layer heated from above (quadrants II and III) will be discussed first. For this situation $\bar{R}_{TC} < 0$ such that it is expected to observe instability in the range $-\infty < \varphi < -1$ for which the overall density gradient ($\partial\rho/\partial y > 0$) is unstable. However, even though the overall density gradient ($\partial\rho/\partial y < 0$) is stable in the range $\varphi > -1$, instability depends strongly on the Lewis number since $\varphi_2 \to 0$ if $Le \to \infty$ and $\varphi_2 \to -1$ (i.e. the instability disappears) if $Le \to 0$. On the other hand, when the layer is heated from below (quadrants I and IV) we have $\bar{R}_T > 0$ such that, according to the linear stability analysis, the system is expected to be stable for $-\infty < \varphi < -1$ and unstable for $\varphi > -1$. The subcritical Rayleigh number, $\bar{R}_{TC}^{sub}$ predicted by the parallel flow approximation (nonlinear theory), (3.14), is presented in quadrant IV, as a dashed line. Below the subcritical Rayleigh number the fluid is expected to remain stable according

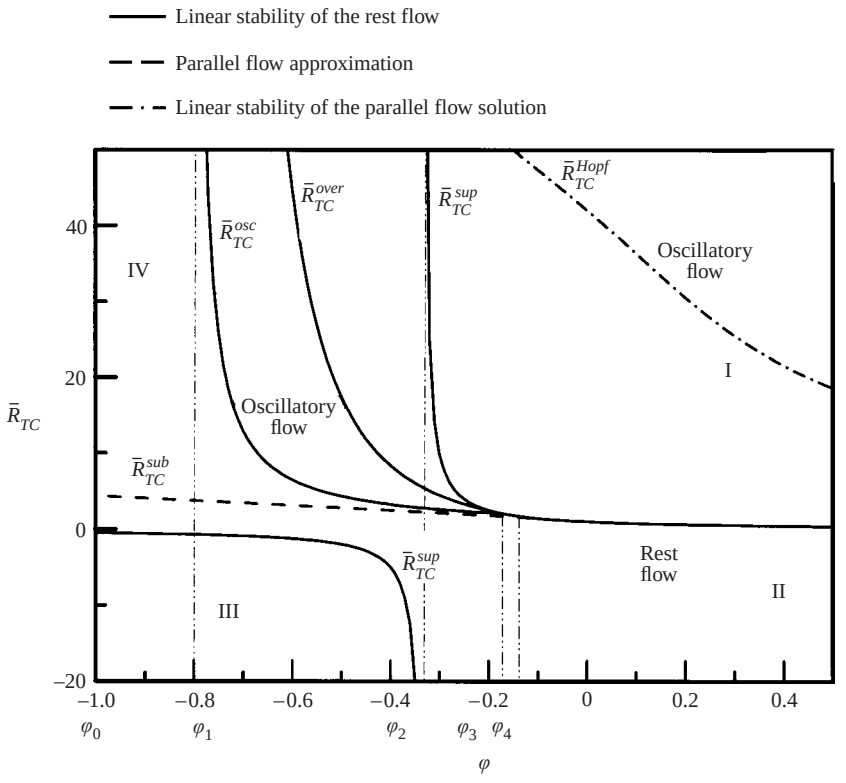

FIGURE 10. Stability diagram in the $(\bar{R}_{TC}, \varphi)$-plane for the case $Le = 2$, $\varepsilon = 0.8$, $a = 1$ and $A \gg 1$ (infinite layer).

to both linear and nonlinear theories. In the region between the subcritical and the overstable Rayleigh numbers the nonlinear theory predicts the possible occurrence of finite-amplitude convection. On the other hand, the rest state is expected to remain stable according to the linear theory. Numerical solutions, obtained in this region, indicate that multiple solutions are indeed possible. Thus, when starting the numerical simulations with a finite-amplitude flow as initial conditions, a convective motion is possible. However the rest state was obtained upon starting the numerical simulation with a very small finite-amplitude flow as initial conditions.

4.2. *Stability of the convective flow*

4.2.1. *Problem formulation*

The finite-amplitude convective flow derived in this study is not expected to remain steady independently of the range of the governing parameters. In fact, it is well known that when the intensity of the flow is increased above a critical value it becomes oscillatory. In order to find this bifurcation point, known as a Hopf bifurcation, a stability analysis of the flow pattern is required. Such an analysis is now discussed.

We consider the parallel flow model described in § 3.2. At the very beginning of instability, the global flow can be assumed to be a superposition of the basic flow $[\Psi(x, y) = \Psi(y), T(x, y) = C_T x + \theta_T(y), S(x, y) = C_S x + \theta_S(y)]$ and an infinitesimal

perturbation that can be developed into normal modes as follows:

$$\left.\begin{aligned}\hat{\Psi}(t,x,y) &= \tilde{\Psi}(y)\,\mathrm{e}^{pt+k(x\cos\Phi+z\sin\Phi)},\\ \hat{\theta}_T(t,x,y) &= \tilde{\theta}_T(y)\,\mathrm{e}^{pt+k(x\cos\Phi+z\sin\Phi)},\\ \hat{\theta}_S(t,x,y) &= \tilde{\theta}_S(y)\,\mathrm{e}^{pt+k(x\cos\Phi+z\sin\Phi)},\end{aligned}\right\} \tag{4.28}$$

where $p=(\sigma+\mathrm{i}\omega)$, σ and ω being, respectively, the perturbation temporal growth rate and frequency. The wavenumber k is real since the system is supposed to be infinite in the horizontal direction and the perturbations are bounded. Φ is the direction of propagation of the travelling waves. Inserting the global flow into the governing equations (2.8)–(2.10) and linearizing about the basic flow state yields the following set of equations:

$$(\mathrm{D}^2-k^2)\tilde{\Psi}+\mathrm{i}k\left(R_T\tilde{\theta}_T+\frac{R_S}{Le}\tilde{\theta}_S\right)=0, \tag{4.29}$$

$$(\mathrm{D}^2-k^2)\tilde{\theta}_T-\mathrm{i}k\mathrm{D}\Psi\tilde{\theta}_T-C_T\mathrm{D}\tilde{\Psi}+\mathrm{i}k\mathrm{D}\theta_T\tilde{\Psi}=p\tilde{\theta}_T, \tag{4.30}$$

$$\frac{1}{Le}(\mathrm{D}^2-k^2)(\tilde{\theta}_S-a\tilde{\theta}_T)-\mathrm{i}k\mathrm{D}\Psi\tilde{\theta}_S-C_S\mathrm{D}\tilde{\Psi}+\mathrm{i}k\mathrm{D}\theta_S\tilde{\Psi}=p\varepsilon\tilde{\theta}_S. \tag{4.31}$$

The corresponding boundary conditions are

$$y=\pm 1/2, \qquad \tilde{\Psi}=0; \qquad \mathrm{D}\tilde{\theta}_T=\mathrm{D}\tilde{\theta}_S=0, \tag{4.32}$$

where $\mathrm{D}=\mathrm{d}/\mathrm{d}y$.

As the system of equations (4.29)–(4.31) contains the basic flow velocity $u(y)=\mathrm{D}\Psi$, we may expect the occurrence of hydrodynamic modes due to destabilization of the velocity profile. For the two-dimensional parallel flow $u(y)$ considered here, the minimum critical unstable R_T occurs for a two-dimensional disturbance propagating in the same direction ($\Phi=0$) (Squire's theorem, see for instance Drazin & Reid 1991).

Also, it is noted that the velocity profile has a point of inflection at $y=0$ with a maximum of $|\mathrm{D}u|$ at the point of inflection. In this configuration the flow is potentially unstable and the hydrodynamic perturbations are developed with an oscillatory mode ($\omega\neq 0$), i.e. giving rise to a Hopf bifurcation. The perturbed state equations (4.29)–(4.31) together with the homogeneous boundary conditions (4.32) may be written in a compact matrix form as

$$\mathscr{L}(k)\boldsymbol{Y}=p\mathscr{M}(k)\boldsymbol{Y}, \tag{4.33}$$

where $\boldsymbol{Y}=[\tilde{\Psi}(y),\tilde{\theta}_T(y),\tilde{\theta}_S(y)]$ is a three-component vector of the perturbation (stream function, temperature and concentration), $\mathscr{L}(k)$ and $\mathscr{M}(k)$ are two linear differential operators that depend on the control parameters R_T, R_S, Le, a and ε.

4.2.2. *Numerical procedure*

The set of equations (4.33) is solved using a finite difference scheme. The system is discretized using a fourth-order scheme in the domain between $y=-1/2$ and $y=1/2$, and written in the form ($\mathscr{L}_{ij}(k)Y_j=p\mathscr{M}_{ij}(k)Y_j$). Using a standard subroutine for eigenvalue problems such as EIGENC of IMSL, the eigenvalues are evaluated as a function of the control parameters R_T, R_S, Le, a, ε and the wavenumber k. For given values of R_S, Le, a and ε, one can determine the value of R_T for which the fastest growth rate (maximal value of σ) cancels out. This gives a functional $R_T=R_T(k,\omega)$. The minimum in the marginal stability curve determines the critical state parameters (k_C,ω_C,R_{TC}). The numerical procedure was found to converge for a discretization number N greater than 100.

	Kimura *et al.* (1995)	Mamou & Vasseur (1999)	Present study
R_{TC}^{Hopf}	506.07	506.07	506.02
k_{TC}^{Hopf}	4.825	4.825	4.825
f_{TC}^{Hopf}	22.11	22.11	22.11

TABLE 1. Comparison of results for pure thermal convection, $R_S = 0$, $a = 0$.

	Mamou & Vasseur (1999)	Present study
R_{TC}^{Hopf}	532.12	532.10
k_{TC}^{Hopf}	4.842	4.831
f_{TC}^{Hopf}	22.73	22.71

TABLE 2. Comparison of results for double-diffusive convection, $R_S = -100$, $a = 0$.

Table 1 shows a comparison between the results predicted by the above numerical procedure and those reported by Mamou & Vasseur (1999) and Kimura, Vynnycky & Alavyoon (1995) for the case of pure thermal convection within an infinite layer. The critical Rayleigh number, the critical wavelength and the corresponding frequency for Hopf bifurcation obtained here are seen to be in excellent agreement with the values reported in the past. In the case of double-diffusive convection, table 2 shows a corresponding comparison for $R_S = -100$, $Le = 10$ and $\varepsilon = 1$.

4.2.3. *Results and discussion*

According to the linear stability analysis discussed above, when the Rayleigh number is increased the unicellular steady convection predicted by the parallel flow approximation eventually becomes unstable. The transition occurs via a Hopf bifurcation at a critical Rayleigh number R_{TC}^{Hopf} which depends upon the value of the governing parameters, namely φ, Le and ε. The effect of these parameters on R_{TC}^{Hopf} is illustrated in figures 11 to 13. For completeness, the critical Rayleigh numbers for the onset of stationary convection (R_{TC}^{sup} and R_{TC}^{sub}) are also included. In these graphs the solid lines correspond to double-diffusive convection and the dashed ones to Soret-induced convection.

Figure 11(a) illustrates the influence of R_S on the critical Rayleigh numbers for $\varepsilon = 1$ and $Le = 2$. The case $R_S = 0$ corresponds to a pure thermal situation for which the onset of stationary convection occurs at a supercritical Rayleigh number $R_{TC}^{sup} = 12$, while the onset of oscillatory convection takes place at a Hopf critical Rayleigh number $R_{TC}^{Hopf} = 506.02$. This last situation has been investigated numerically by Kimura *et al.* (1995), for horizontal shallow cavities. They found that for a given aspect ratio A of the layer it was difficult to ascertain the exact value of R_{TC}^{Hopf}. Further, as expected, their results indicate that R_{TC}^{Hopf} depends on A. Thus they found that R_{TC}^{Hopf} lies between 730 and 750 for $A = 4$ but decreases to somewhere between 630 and 650 for $A = 8$. With the numerical code used here it was found that $600 < R_{TC}^{Hopf} < 650$ when $A = 8$. The case $R_S > 0$, for which the solutal buoyancy forces are destabilizing, is now discussed. For this situation the onset of stationary convection occurs through a pitchfork bifurcation predicted by (3.13). Thus $R_{TC}^{sup} > 0$ ($R_{TC}^{sup} < 0$) for $R_S < 12/(1 + 0.5a)$ ($R_S > 12/(1 + 0.5a)$). Similarly, R_{TC}^{Hopf} is observed to

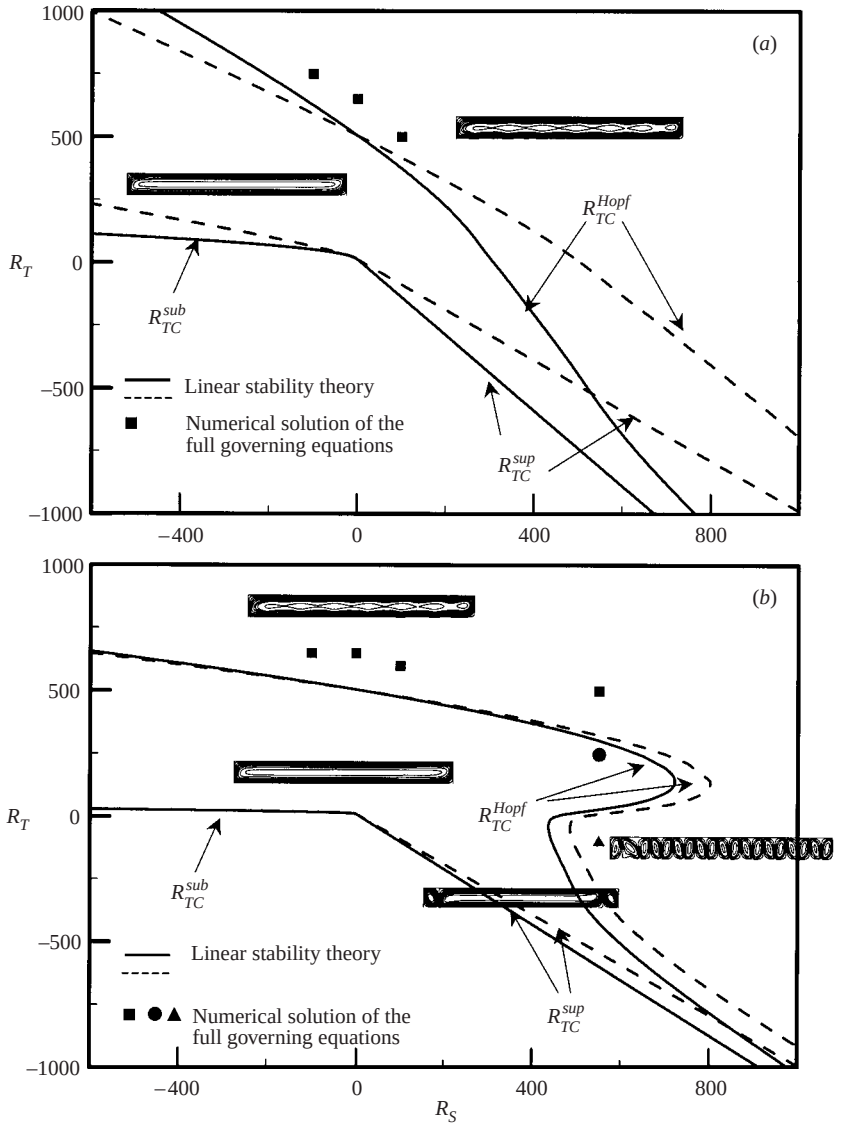

FIGURE 11. Critical Rayleigh number for Hopf bifurcation R_{TC}^{Hopf} for $\varepsilon = 1$, in terms of R_S for (*a*) $Le = 2$ and (*b*) $Le = 10$. Solid line, Soret-driven convection; dashed line, double-diffusive convection.

be > 0 for $R_S < 505$ when $a = 0$ and $R_S < 308$ when $a = 1$. Above these values the critical Rayleigh numbers for the onset of the oscillating convection are negative. Further, it is observed that, in the case of Soret-driven convection, the range of possible existence of a steady parallel flow ($R_{TC}^{sup} < R_T < R_{TC}^{Hopf}$) becomes smaller and smaller as the value of R_S is increased. This trend is similar in the case of double-diffusive convection, although the range of existence of a parallel flow is observed to be larger. On the other hand, for $R_S < 0$, i.e. when the solutal buoyancy forces are stabilizing, the onset of stationary convection corresponds to a subcritical bifurcation predicted by (3.14). Naturally, both R_{TC}^{sub} and R_{TC}^{Hopf} must be > 0 for this situation. Figure 11(*a*) indicates that, except for R_{TC}^{Hopf} in the $R_S < 0$ region, the Soret-induced

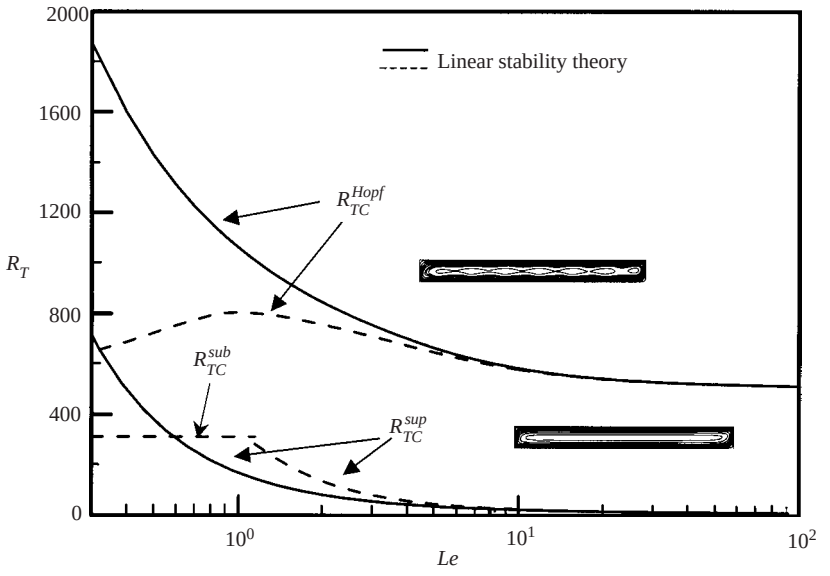

FIGURE 12. Critical Rayleigh number for Hopf bifurcation R_{TC}^{Hopf} in terms of Le for $\varepsilon = 1$ and $R_S = -100$. Solid line, Soret-driven convection; dashed line, double-diffusive convection.

convection is less stable than the double-diffusive convection. Also the results indicate that, for both Soret-driven and double-diffusive convection, the range of possible existence of a parallel flow is increased as the value of R_S is made larger.

A few numerical results are also presented in figure 11(a). For the set of governing parameters considered these, two different flow patterns were obtained. The first one, in the zone between R_{TC}^{Hopf} and R_{TC}^{sup} or R_{TC}^{sub}, corresponds to a steady parallel flow. The second one, in the zone above R_{TC}^{Hopf}, corresponds to a superposition of a parallel flow structure, near the walls of the cavity, and small travelling cells in the core of the enclosure. This flow pattern is similar to that presented in figure 14(c). Figure 11(b) shows the results obtained for $Le = 10$. It is observed that, upon increasing Le from 2 to 10, the difference between the results predicted for double-diffusive convection and Soret-induced convection becomes very small. This point is illustrated in figure 12 which shows the effect of the Lewis number on the critical Rayleigh numbers R_{TC}^{sub}, R_{TC}^{sup} and R_{TC}^{Hopf} for the case $R_S = -100$ and $\varepsilon = 1$. For $Le < 1$, a large difference is observed between the results obtained for $a = 0$ and $a = 1$. However, figure 12 indicates clearly that this difference decreases considerably for $Le > 1$ and becomes negligible for $Le \geqslant 10$.

Another effect of the Lewis number is depicted in figure 11(b). The behaviour of the R_{TC}^{Hopf} curve, in the $R_S > 0$ region, indicates the formation of a Z-shape. This implies that, in this region, for a given R_S two different solutions are possible for R_{TC}^{Hopf}. The numerical results obtained for this situation were essentially similar to those reported for $Le = 2$. Thus, for $R_S = 550$, it was found that for $R_T = 500$ the streamlines correspond to a superposition of a parallel flow and travelling waves. For $R_T = 250$ the flow was observed to be steady and parallel. However, in the Z-zone, for $R_T = -100$ a multicellular flow pattern was obtained. Furthermore, the numerical results indicate that this flow is slightly oscillating. Finally, in the zone between R_{TC}^{sub} and R_{TC}^{Hopf}, in the region $R_S > 0$ and $R_T < 0$, a multicellular flow is obtained. This consists of a parallel

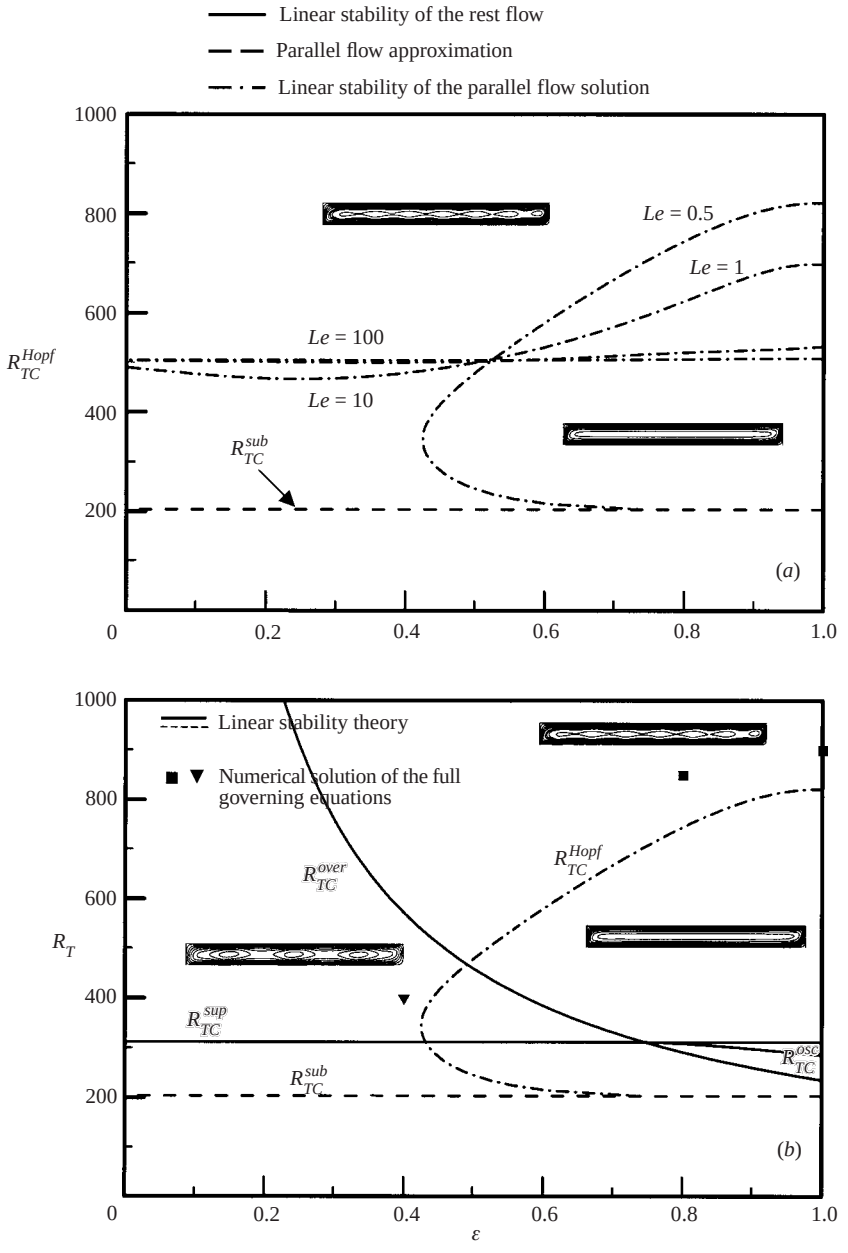

FIGURE 13. (*a*) Critical Rayleigh number for Hopf bifurcation R_{TC}^{Hopf} as a function of ε for $R_S = -100$, $a = 1$ and $Le = 0.5$, 1, 5 and 10. (*b*) Various critical Rayleigh numbers for $Le = 0.5$.

flow in the core of the cavity, and two small vortices near the vertical boundaries, as already observed in figure 6.

Figure 13(*a*) shows the influence of the normalized porosity, ε, on R_{TC}^{Hopf} in the case of Soret-induced convection for $R_S = -100$ and various values of Le. In general it is observed that the onset of oscillating flow (R_{TC}^{Hopf}) decreases considerably as the value of the normalized porosity, ε, is made smaller. Consequently, the steady parallel flow is destabilized earlier with a decrease of ε. This effect is more important for

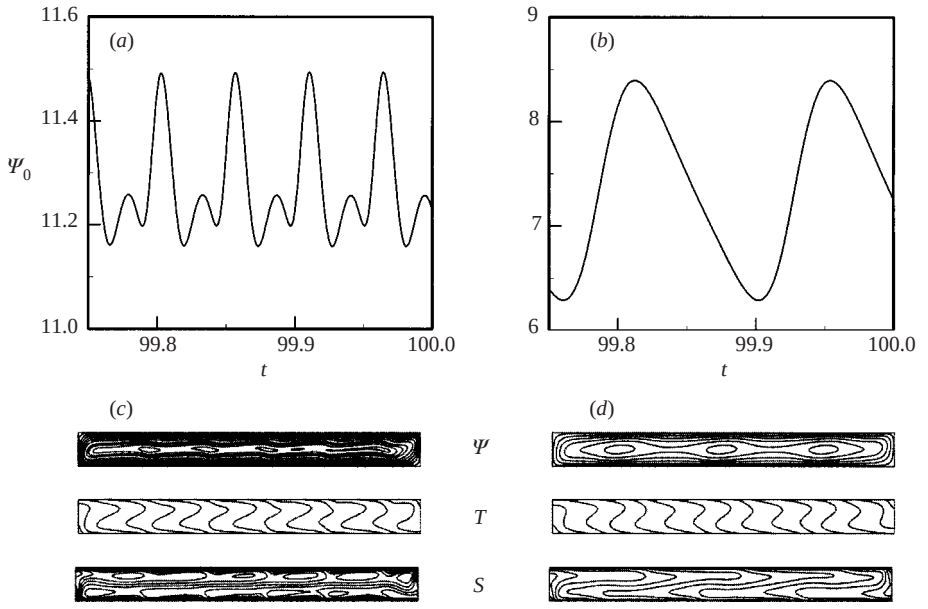

FIGURE 14. (a, b) Time history of the stream function extrema obtained for $R_T = 800$, $R_S = -100$, $Le = 0.5$, $A = 10$, $a = 1$ and (a) $\varepsilon = 0.8$, (b) $\varepsilon = 0.4$. (c, d) Streamline, temperature and solute contours at given time t for (c) $\varepsilon = 0.8$ and (d) $\varepsilon = 0.4$.

small Lewis numbers. For a Lewis number equal to one, R_{TC}^{Hopf} depends significantly upon ε. However, this dependence is observed to become negligible for $Le \geqslant 10$. For $Le = 0.5$ the linear stability theory predicts that Hopf bifurcations are not possible for values of ε smaller than 0.43. For this situation, the steady parallel flow solution is no longer possible. In fact, the numerical results indicate that the onset of convection, from the rest flow, occurs directly through an oscillating flow. A steady parallel flow regime is not possible for this situation. On the other hand, for $\varepsilon > 0.43$, the results indicate the existence of two possible R_{TC}^{Hopf} for a given value of ε. Another view of the results obtained for the case $Le = 0.5$ is presented in figure 13(b). The critical Rayleigh numbers, predicted by the linear stability theory, namely R_{TC}^{sup}, R_{TC}^{over} and R_{TC}^{osc}, as predicted by (4.13), (4.14), and (4.15) respectively, are depicted in the graph. The critical Rayleigh numbers for the onset of subcritical convection, predicted by the parallel flow theory, (3.14), are also presented. Typical streamlines obtained from the numerical simulations are presented in figure 13. They are observed to be similar to those discussed in figure 11(a, b).

Figure 14(a, b) shows the time history of Ψ_0 obtained numerically for the case $R_T = 800$, $R_S = -100$, $a = 1$, $Le = 0.5$, $A = 10$ and $\varepsilon = 0.8$ and 0.4 respectively. For $\varepsilon = 0.8$ the numerical results indicate the existence of small vortices in the core of the cavity travelling from right to the left. Typical streamlines obtained from the numerical simulations at a given time t are presented in figure 14(c, d). The time evolution of Ψ_0, for this situation, is depicted in figure 14(a). This oscillating motion is composed of two fundamental peaks. For $\varepsilon = 0.4$, it was found numerically that the flow pattern consists of a combination of a parallel flow and small cells in the core of the cavity travelling horizontally forward and backward around a given position; this oscillating motion is of a single frequency. Figure 14(d) shows the streamlines, isotherms and isoconcentrations for $\varepsilon = 0.4$.

5. Conclusion

In this paper an analytical and numerical study of natural convection in a horizontal porous layer filled by a binary fluid is carried out. The case of Soret-driven convection ($a = 1$) is compared with the case of double-diffusion convection ($a = 0$) discussed by Mamou & Vasseur (1999). The linear stability theory has been used to predict the marginal state of instability via stationary convection or oscillatory motions. Analytical solutions, for finite-amplitude convection, are derived on the basis of the parallel flow approximation for a shallow enclosure. The critical Rayleigh numbers for the onset of supercritical and subcritical convection are predicted by this theory. The stability of the parallel flow solution is studied and the threshold for Hopf bifurcation is determined. The governing parameters of the problem are the thermal Rayleigh number R_T, buoyancy ratio φ, Lewis number Le, normalized porosity of the porous medium ε, aspect ratio of the layer A, and the type of convection (i.e. parameter a) considered.

The main conclusions of the present analysis are as follows:

(i) The stability of the motionless regime has been studied analytically on the basis of both the linear and nonlinear perturbation theories. The linear model shows that in the $(\bar{R}_T, \varphi)$-space the type of the first primary bifurcation (stationary or oscillatory) depends only on Le, ε and a. The critical Rayleigh numbers for the onset of supercritical, overstable and oscillatory convections have been obtained in terms of those parameters. In the case $Le \gg 1$ the results are found to be independent of a, i.e. of the type of convection considered.

(ii) An analytical solution, based on the parallel flow approximation, has been derived for the case of an infinite layer ($A \gg 1$). The resulting nonlinear model yields the supercritical Rayleigh number for the onset of convection from the rest state. For opposing buoyancy forces ($\varphi < 0$) the model predicts the existence of a subcritical branch, where the flow bifurcates from the rest state through finite-amplitude convection. An explicit expression for the subcritical Rayleigh number is obtained in terms of φ , Le and a. For finite-amplitude convection, useful expressions have been obtained for velocity, temperature and solute distributions in the core of the layer. The influence of governing parameters on the Nusselt and Sherwood numbers are predicted and discussed. The main features predicted by the analytical solution are confirmed by numerical solutions of the full governing equations.

(iii) The stability of the flows, predicted by the analytical model (parallel flow approximation), has been investigated. The onset of oscillatory convection (Hopf bifurcation) has been obtained numerically on the basis of the linear stability theory. It has been found that the critical Rayleigh number for the onset of Hopf bifurcation depends upon φ, Le, ε and a. Here again, for $Le \gg 1$, R_{TC}^{Hopf} is found to be independent of a. The frequency of oscillations predicted by linear analysis has been found, for several sets of dimensionless parameters, to be in good agreement with the results of the numerical simulations of the full governing equations.

REFERENCES

Bejan, A. & Tien, C. L. 1978 Natural convection in a horizontal porous medium subjected to an end-to-end temperature difference. *J. Heat Mass Transfer* **100**, 191–198.

Bergeron, A., Henry, D., BenHadid, N. & Tuckerman, L. S. 1998 Marangoni convection in binary mixtures with Soret effect. *J. Fluid Mech.* **375**, 143–177.

Blythe, P. A., Daniels, P. G. & Simpkins, P. G. 1985 *Limiting Behaviours in Porous Media Cavity: Fundamentals and Applications.* pp. 600–611. Hemisphere.

Brand, H. R. & Steinberg, V. 1983*a* Convective instabilities in binary mixtures in a porous medium. *Physica* **119A**, 327–338.

Brand, H. R. & Steinberg, V. 1983*b* Nonlinear effects in the convective instability of a binary mixture in a porous medium near threshold. *Phys. lett.* **93A**, 333–336.

Chen, F. & Chen, C. F. 1993 Double diffusive fingering convection in a porous medium. *Intl J. Heat Mass Transfer* **36**, 793–807.

Daniels, P. G., Simpkins, P. G. & Blythe, P. A. 1989 Thermally driven shallow cavity flows in porous media: the merged layer regime. *Proc. R. Soc. Lond.* A **426**, 107–124.

De Groot, S. R. & Mazur, P. 1962 *Non Equilibrium Thermodynamics*. North Holland.

Drazin, P. G. & Reid, W. H. 1991 *Hydrodynamic Stability*. Cambridge University Press.

Joseph, D. D. 1976 *Stability of Fluid Motion I and II*. Springer.

Kimura, S., Vynnycky, M. & Alavyoon, F. 1995 Unicellular natural circulation in a shallow horizontal porous layer heated from below by a constant flux. *J. Fluid Mech.* **294**, 231–257.

Malashetty, M. S. 1993 Anisotropic thermoconvective effects on the onset of double diffusive convection in a porous medium. *Intl J. Heat Mass Transfer* **39**, 2397–2401.

Mamou, M. & Vasseur, P. 1999 Thermosolutal bifurcation phenomena in porous enclosures subject to vertical temperature and concentration gradients. *J. Fluid Mech.* **395**, 61–87.

Mamou, M., Vasseur, P., Bilgen, E. & Gobin, D. 1995 Double-diffusive convection in an inclined slot filled with porous medium. *Eur. J. Mech.* B/*Fluids* **14**, 629–652.

Nield, D. A. 1967 The thermohaline Rayleigh-Jeffreys problem. *J. Fluid Mech.* **29**, 545–558.

Ouarzazi, M. N. & Bois, P. A. 1994 Convective instability of a fluid mixture in a porous medium with time-dependent temperature. *Eur. J. Mech.* B/*Fluids.* **13**, 275–298.

Patankar, S. V. 1980 *Numerical Heat Transfer and Fluid Flow*. Hemisphere.

Platten, J. K. & Legros, J. C. 1984 *Convection in Liquids*. Springer.

Poulikakos, D. 1986 Double diffusive convection in a horizontal sparcely packed porous layer. *Intl Commun. Heat Mass Transfer* **13**, 587–598.

Rudraiah, N., Shrimani, P. K. & Friedrich, R. 1982*a* Finite amplitude thermohaline convection in a fluid saturated porous layer. *7th Intl Heat Transfer Conf. Münich* (ed. U. Griguff, E. Hahn, K. Stephan & J. Straub). Hemisphere.

Rudraiah, N., Shrimani, P. K. & Friedrich, R. 1982*b* Finite Amplitude convection in a two-component fluid saturated porous layer. *Intl J. Heat Mass Transfer* **25**, 715–722.

Sovran, O., Charrier-Mojtabi, M. C. & Mojtabi, A. 2001 Naissance de la convection thermo-solutale en couche poreuse infinie avec effet Soret. *C. R. Acad. Sci. Paris* **329** 11b, 287–293.

Taslim, M. E. & Narusawa, U. 1986 Binary fluid convection and double-diffusive convection in porous medium. *J. Heat Transfer* **108**, 221–224.

Taunton, J. W., Lightfoot, E. N. & Green, T. 1972 Thermohaline instability and salt fingers in a porous medium. *Phys. Fluids* **15**, 748–753.

Trevisan, O. V. & Bejan, A. 1987 Mass and heat transfer by high Rayleigh number convection in a porous medium heated from below. *Intl J. Heat Transfer* **30**, 2341–2356.

Walker, K. L. & Homsy, G. M. 1978 Convection in a porous cavity. *J. Fluid Mech.* **87**, 449–474.